Marked enhancement of the photoresponsivity and minority-carrier lifetime of BaSi2 passivated with atomic hydrogen

doi: 10.1103/PhysRevMaterials.3.065403

Marked enhancement of the photoresponsivity and minority-carrier lifetime of $BaSi_2$ passivated with atomic hydrogen

Zhihao Xu,[1] Denis A. Shohonov,[2] Andrew B. Filonov,[2] Kazuhiro Gotoh,[3] Tianguo Deng,[1] Syuta Honda,[4] Kaoru Toko,[1] Noritaka Usami,[3] Dmitri B. Migas,[2,5] Victor E. Borisenko,[2,5] and Takashi Suemasu[1,*]

[1]*Institute of Applied Physics, University of Tsukuba, Tsukuba, Ibaraki 305-8573, Japan*
[2]*Department of Micro- and Nanoelectronics, Belarusian State University of Informatics and Radioelectronics, P. Brovki 6, 220013 Minsk, Belarus*
[3]*Graduate School of Engineering, Nagoya University, Nagoya 464-8603, Japan*
[4]*Department of Pure and Applied Physics, Faculty of Engineering Science, Kansai University, Suita 564-8680, Japan*
[5]*National Research Nuclear University MEPhI (Moscow Engineering Physics Institute), Kashirskoe Shosse 31, 115409 Moscow, Russia*

* Corresponding author at:
Institute of Applied Physics, Faculty of Pure and Applied Sciences, University of Tsukuba, Tsukuba, Ibaraki 305-8573, Japan
*Electronic mail: suemasu@bk.tsukuba.ac.jp

Passivation of barium disilicide ($BaSi_2$) films is very important for their use in solar cell applications. In this paper, we demonstrated the effect of hydrogen (H) passivation on both the photoresponsivity and minority-carrier lifetime of $BaSi_2$ epitaxial films grown by molecular beam epitaxy. First, we examined the growth conditions of a 3 nm-thick hydrogenated amorphous silicon (a-Si) capping layer formed on a 500 nm-thick $BaSi_2$ film and found that an H supply duration ($t_{a\text{-}Si:H}$) of 15 min at a substrate temperature of 180 °C sizably enhanced the photoresponsivity of the $BaSi_2$ film. We next supplied atomic H to $BaSi_2$ epitaxial films at 580 °C and changed supply duration ($t_{BaSi:H}$) in the range of 1–30 min, followed by capping with an a-Si layer. The photoresponsivity of the films changed considerably depending on $t_{BaSi:H}$ and reached a maximum of 2.5 A/W at a wavelength of 800 nm for the sample passivated for $t_{BaSi:H}$ =15 min under a bias voltage of 0.3 V applied to the front-surface indium-tin-oxide electrode with respect to the back-surface aluminum electrode. This photoresponsivity is approximately one order of magnitude higher than the highest value previously reported for $BaSi_2$. Microwave photoconductivity decay measurements revealed that the minority-carrier lifetime of the $BaSi_2$ film with the highest photoresponsivity was 14 μs, equivalent to its bulk carrier lifetime ever reported. We performed theoretical analyses based on a rate equation including several recombination mechanisms and reproduced the experimentally obtained decay curves. We also calculated the total density of states of $BaSi_2$ by *ab initio* studies when one Si vacancy existed in a unit cell and one, two, and three H atoms occupied Si vacancy or interstitial sites. A Si vacancy caused a localized state with two energy bands to appear close to the middle of the band gap. In certain cases, H passivation of the Si dangling bonds can markedly decrease trap concentration. From both experimental and theoretical viewpoints, we conclude that an atomic H supply is beneficial for $BaSi_2$ solar cells.

I. INTRODUCTION

Over the past decade, thin film solar cell materials such as copper indium gallium selenide ($CuIn_{1-x}Ga_xSe_2$, CIGS) and cadmium telluride (CdTe) have attracted increasing attention because of their low cost and high conversion efficiencies (η). The highest η of CIGS and CdTe solar cells currently exceeds 22% [1]. However, these materials contain toxic and/or scare elements. Thus, it is important to explore alternative materials for use in solar cells. Solar cell materials should be safe, stable, and earth-abundant, like silicon (Si). Furthermore, materials with a large absorption coefficient (α), suitable band gap, and superior minority-carrier properties are desirable to achieve high η. Among such materials, we have paid considerable attention to semiconducting barium disilicide ($BaSi_2$). $BaSi_2$ possesses all of these properties [2,3], such as a band gap of 1.3 eV, large α of 3×10^4 cm^{-1} at 1.5 eV [4-7], and excellent bulk minority-carrier lifetime (τ) of 14 μs for thin-film solar cell applications because of its inactive grain boundaries [8,9]. $BaSi_2$ can be grown epitaxially on a Si substrate [10,11] and its band gap can be increased by adding other elements such as Sr and C [12,13]. Therefore, $BaSi_2$ is a material of choice aiming for $\eta > 30\%$ in a Si-based tandem-structure solar cell. As a first step, we chose to form p-$BaSi_2$/n-Si heterojunction solar cells, and have achieved η approaching 10% [14,15]. In a p-$BaSi_2$/n-Si solar cell, however, the built-in potential is as small as 0.2 V because of the low electron affinity of $BaSi_2$ (3.2 eV) [16]. The experimentally obtained open-circuit voltage was thus smaller than 0.5 V, limiting the η. Hence, we next moved on to $BaSi_2$ homojunction solar cells, and recently demonstrated the operation of a homojunction solar cell capped with an amorphous silicon (a-Si) layer [17,18]. To achieve high η in a homojunction solar cell, the formation of high-quality $BaSi_2$ light absorber layer is very important.

Currently, we are focusing on further improvement of the minority-carrier properties of $BaSi_2$ absorber layers grown by molecular beam epitaxy (MBE). In particular, photoresponsivity is a decisive minority-carrier parameter that strongly affects η. Recently, we found that the photoresponsivity, carrier type, and carrier concentration of $BaSi_2$ absorber layers are fairly sensitive to the ratio of Ba deposition rate to Si deposition rate (R_{Ba}/R_{Si}) during MBE growth [19]. The maximum photoresponsivity was obtained at around $R_{Ba}/R_{Si} = 2.2$ when $BaSi_2$ films are grown at 580 °C. However, electrically active defect levels were detected even in such a $BaSi_2$ film by deep-level transient spectroscopy [20]. The defect density of this film was of the order of 10^{13} cm^{-3}. The carrier filling properties of the film indicated that the detected defect levels probably originated from Si vacancies (V_{Si}) in $BaSi_2$ [20]. In a unit cell of $BaSi_2$, there are four distinct Si tetrahedra, as shown in Fig. 1. In each Si tetrahedron, one Si atom is bonded covalently to three other Si atoms [21,22]. Kumar *et al*.

performed a first-principles calculation that suggested that V_{Si} are most likely to occur as point defects in $BaSi_2$ regardless of whether the growth conditions are rich or poor in Si [22]. The calculation also revealed that V_{Si} generate dangling bonds and thereby localized states within the band gap, leading to the degradation of the minority-carrier properties of $BaSi_2$. Therefore, it is of particular importance to passivate these active defects in the bulk of $BaSi_2$ films.

We also have to consider defects in the surface region of $BaSi_2$. The bond configuration changes abruptly at the $BaSi_2$ surface. According to an analysis of the surface structure of $BaSi_2$ epitaxial layers using coaxial-collision ion scattering spectroscopy conducted by Katayama *et al.*, an *a*-axis-oriented $BaSi_2$ epitaxial film is terminated by Si_4 tetrahedra [23,24]. Therefore, surfaces can contain very high densities of trap states in the band gap [25]. Such surface defects deteriorate solar cell performance because short-wavelength light is absorbed close to the surface. Therefore, surface passivation is very important for materials like $BaSi_2$ that possess large α. Of course, not only defects in the surface region but also those in bulk and interface regions have to be considered for photogenerated carriers on their way to the electrode.

Passivation with hydrogen (H) is often conducted when the density of Si dangling bonds should be kept as low as possible [26] and is also used in state-of-the-art heterojunctions with intrinsic thin-layer solar cells [27,28]. In our previous papers, we found that capping a $BaSi_2$ film with a 3 nm-thick hydrogenated a-Si layer (a-Si:H) formed using radio-frequency (RF) plasma enhanced the photoresponsivity of $BaSi_2$ by approximately 4 times compared with that of a $BaSi_2$ layer capped with a pure a-Si layer [29,30]. However, the growth conditions of a-Si:H on $BaSi_2$ have yet to be optimized.

In this paper, we first optimize the formation of a-Si:H capping layers for $BaSi_2$ from the viewpoint of photoresponsivity. We next investigate the effect of atomic H supply on the photoresponsivity enhancement of $BaSi_2$ films. Atomic H is supplied to $BaSi_2$ films prior to the formation of a-Si capping layers and their photoresponsivity is measured. The τ values of the films are also evaluated. We analyze the experimentally obtained decay curves by considering several trap-related recombination mechanisms, and perform *ab initio* calculations to verify the effect of H passivation on $BaSi_2$ films.

II. METHODS

A. Formation and characterization of $BaSi_2$ films capped with a-Si layers

We used an ion-pumped MBE system equipped with a standard Knudsen cell for Ba, an electron-beam gun for Si, and an RF plasma generator for atomic H. First, Ba and Si atoms were co-deposited on a low-resistivity (ρ) Czochralski-grown (CZ) n^+-Si(111) substrate (ρ = 0.01 Ωcm) at a substrate temperature (T_S) of 580 °C to form a $BaSi_2$ epitaxial film with a thickness of approximately 500 nm, followed by a 3

nm-thick a-Si capping layer. We also used the low-ρ CZ n^+-Si(111) substrates for photoresponse measurements to exclude the contribution of photogenerated carriers in the n-Si substrate and form a good electrical contact at the $BaSi_2$/Si heterointerface. For samples A−C, we formed a-Si capping layers at T_S = 180 °C and supplied atomic H for different durations $t_{a\text{-}Si:H}$ of 1, 15, and 30 min at T_S = 180 °C. For samples D−H, we formed a-Si layers at various T_S (160−260 °C), and supplied atomic H at the same T_S for $t_{a\text{-}Si:H}$ = 15 min. We set the RF power at 70 W and vacuum level at 10^{-3} Pa during atomic H supply. Details of samples are summarized in Table I. Formation of Si-H bonds in a-Si:H layers was confirmed by Raman spectroscopy in our previous report [30]. Raman spectra were recorded by a Raman spectrometer (JASCO, NRS-5100) using a frequency-doubled Nd:YAG laser (532 nm, 5.1 mW). The spectral resolution was better than 4.2 cm^{-1}.

TABLE I. Structure, substrate temperature (T_S), H supply duration ($t_{a\text{-}Si:H}$) for 3 nm-thick a-Si:H layers. The $BaSi_2$ layers (500 nm) were grown at 580 °C.

Structure	Sample	T_S (°C)	$t_{a\text{-}Si:H}$ (min)
a-Si:H/$BaSi_2$(500 nm)/n^+-Si	A	180	1
	B	180	15
	C	180	30
	D	160	15
	E	170	15
	F	190	15
	G	210	15
	H	260	15

We next investigated the effect of atomic H on 500 nm-thick $BaSi_2$ epitaxial films. 500 nm-thick $BaSi_2$ films were grown epitaxially at T_S = 580 °C on the low-ρ CZ n^+-Si(111) substrates (ρ = 0.01 Ωcm), and then atomic H was supplied to the $BaSi_2$ films with different durations $t_{BaSi:H}$ at T_S = 580 °C for samples 1–5 and at T_S = 180 °C for sample 6. After that, a 3 nm-thick pure a-Si capping layer was deposited at T_S = 180 °C in samples 1–6. A reference sample, a 500 nm-thick $BaSi_2$ epitaxial film grown at T_S = 580 °C on the low-ρ CZ n^+-Si(111) substrate with a pure a-Si capping layer, was also fabricated and subjected to photoresponse measurements. The vacuum level and RF power of the H plasma generator were set at 10^{-3} Pa and 10 W, respectively, to prevent surface damage. τ was measured for samples 7–9 grown on floating-zone (FZ) n-Si (111) substrates with high ρ (> 1000 Ωcm) by a microwave photoconductivity

decay (μ−PCD) measurement system (Kobelco, LTA-1512EP). Sample preparation for photoresponse and μ−PCD measurements is summarized in Table II. We also grew approximately 300 nm-thick $BaSi_2$ films at T_S = 580 °C with different durations $t_{BaSi:H}$ = 0, 9, 15, and 30 min for the depth profile of H atoms by secondary ion mass spectrometry (SIMS) using 5.0-kV Cs^+ primary ions.

For the photoresponse measurements, 80 nm-thick indium tin oxide (ITO) electrodes with a diameter of 1 mm were fabricated by sputtering onto the front sides of the wafers and 150 nm-thick Al layers were deposited on the back sides of the wafers. Photoresponse spectra were collected under bias voltages between the front and back electrodes by a lock-in technique using a xenon lamp (Bunko Keiki, SM- 1700A) and a single monochromator with a focal length of 25 cm (Bunko Keiki, RU-60N). The photoresponsivity R [A/W] for a given wavelength was obtained as follows. The alternating current components J [A/cm^2] caused by chopped light illuminations P [W/cm^2] was measured on samples under bias voltages between the top and bottom electrodes by a lock-in technique. The R is given by J/P, and was measured from 300 to 1200 nm at an interval of 20 nm. The light intensity of the lamp was calibrated using a pyroelectric sensor (Melles Griot, 13PEM001/J). The crystalline quality of the grown films was characterized by x-ray diffraction (XRD; Rigaku Smart Lab) using Cu Kα radiation. The out-of-plane and in-plane XRD measurements revealed the *a*-, *b*- and *c*-axis lattice constants (*a*, *b*, and *c*) using the Nelson-Riely relationship [31]. Ge(220) single crystals were set to monochromatize the x-ray beam. All measurements were performed at room temperature (RT).

TABLE II. Structure, H supply duration ($t_{BaSi:H}$), and substrate temperature (T_S) for 500 nn-thick $BaSi_2$ epitaxial layer growth of samples used to measure minority-carrier lifetimes. Pure a-Si capping layers (3 nm thick) were deposited at 180 °C.

	Sample	$t_{BaSi:H}$ (min)	T_S (°C)
a-Si /$BaSi_2$:H/n^+-Si	1	1	580
	2	10	580
	3	15	580
	4	20	580
	5	30	580
	6	15	180
	Reference	0	580
a-Si /$BaSi_2$:H/n-Si	7	1	580
	8	15	580
	9	30	580

B. Computational details

We calculated the electronic properties of various $BaSi_2$ structures with V_{Si} and different numbers of incorporated H atoms. The full structural optimization and density of states (DOS) calculations of the 2 × 3 × 2 increased unit cell of $BaSi_2$ with and without H incorporation were performed by the first-principles total energy projector-augmented wave method (VASP code) [32-34] with a plane-wave basis set. The generalized gradient approximation of Perdew–Burke–Ernzerhof [35] was used for the exchange and correlation potentials. Total energy minimization, via optimization of lattice parameters and relaxation of atomic positions using a conjugate gradient routine, was obtained by calculating the Hellmann–Feynman forces and stress tensor. Pulay corrections were included to compensate for changes of the basis set caused by variation in the shape of the unit cell. We set the energy cutoff at 325 eV. To perform integration over the Brillouin zone, we used a 5 × 5 × 5 mesh of Monkhorst–Pack points, which was found to be sufficient to obtain convergence in the total energy of less than 0.001 eV per unit cell. The atomic relaxation was stopped when forces on the atoms were smaller than 0.05 eV/Å. Total DOS were calculated by the tetrahedron method with Blöchl corrections.

III. RESULTS AND DISCUSSION

A. Optimal growth conditions of a-Si:H passivation layers

Figure 2(a) shows the photoresponse spectra of samples A−C. The a-Si:H layers of those samples were formed at T_S = 180 °C for $t_{a\text{-}Si:H}$ of 1, 15, and 30 min, respectively. Since there was no built-in electric field in the $BaSi_2$ films, a bias voltage of 0.3 V was applied to the ITO electrode with respect to the Al electrode so that the photogenerated electrons were extracted to the front ITO electrode. The photoresponsivity began to increase at wavelengths (λ) shorter than approximately 1000 nm, corresponding to the band gap of $BaSi_2$. The smallest photoresponsivity was obtained for sample A fabricated with the shortest $t_{a\text{-}Si:H}$ (1 min). The photoresponsivity improved considerably by increasing $t_{a\text{-}Si:H}$ to 15 min (sample B). The photoresponsivity of sample B exceeded 1.4 A/W at λ = 800 nm. However, a further increase of $t_{a\text{-}Si:H}$ to 30 min (sample C) led to decreased photoresponsivity. We speculate that part of the a-Si capping layer changed to the crystalline Si phase when $t_{a\text{-}Si:H}$ = 30 min, and thus the passivation effect of the capping layer degraded. Sriraman *et al.* investigated H-induced crystallization of a-Si upon exposure to H through a combination of molecular-dynamics simulations and *in situ* attenuated total-reflection Fourier transform infrared spectroscopy [36]. We therefore chose $t_{a\text{-}Si:H}$ = 15 min and optimized T_S between 160 and 260 °C to prevent crystallization of a-Si by annealing [37, 38]. The photoresponse spectra of samples B and D–H formed with $t_{a\text{-}Si:H}$ = 15 min and various T_S are shown in Fig. 2(b). The

photoresponsivity was the highest for sample B (T_S = 180 °C) and was lower for samples produced using either higher or lower T_S. These results indicate that the optimal growth conditions of an a-Si:H capping layer are $t_{a\text{-}Si:H}$ = 15 min and T_S = 180 °C.

B. Properties of H-passivated $BaSi_2$

Figure 3 shows the photoresponse spectra of samples 1–6 and the reference sample under a bias voltage of 0.3 V. For samples 1–5, H atoms were irradiated on 500 nm-thick $BaSi_2$ films at T_S = 580 °C for various $t_{BaSi:H}$ of 1 to 30 min after the growth of $BaSi_2$ films at T_S = 580 °C. For sample 6, T_S was set at 180 °C and $t_{BaSi:H}$ was 15 min. Photoresponsivity increased with $t_{BaSi:H}$ up to 15 min and then decreased as $t_{BaSi:H}$ lengthened further. This behavior is caused by the passivation of defects in $BaSi_2$ by the atomic H. The maximum photoresponsivity of about 2.5 A/W at λ = 800 nm was observed for sample 3 ($t_{BaSi:H}$ = 15 min). This value is approximately one order of magnitude higher than that reported previously [30], and much larger than that of sample B [see Fig. 2(a)]. The photoresponsivities of samples 2 ($t_{BaSi:H}$ = 10 min) and 3 ($t_{BaSi:H}$ = 15 min) were almost the same at λ < 500 nm. This behavior is believed to originate from saturation of passivated defects on the top surfaces of these samples. Photons with λ < 500 nm were absorbed in the region close to the surface of the $BaSi_2$ films because of the large absorption coefficient of $BaSi_2$. Therefore, the results suggest that the recombination of photogenerated carriers is suppressed in the $BaSi_2$ films, especially in the surface region. Improved photoresponsivity compared with that of the reference sample was distinctly observed at λ > 500 nm for samples 1–3. We suppose that the H atoms might diffuse into deeper regions and passivate the defects in the bulk of $BaSi_2$. The photoresponsivity of the samples decreased markedly when $t_{BaSi:H}$ was longer than 15 min. The reason for this is discussed later. Comparing the photoresponsivities of sample 6 ($t_{BaSi:H}$ = 15 min and T_S = 180 °C) and sample 3 ($t_{BaSi:H}$ = 15 min and T_S = 580 °C) indicates that the photoresponsivity improvement is independent of T_S. We speculate that H atoms diffuse sufficiently in $BaSi_2$ even at the low T_S. In other words, the diffusion coefficient of H in $BaSi_2$ is large at low temperature. In monocrystalline Si, the diffusion coefficient of H is large even at low temperatures [39]. These results provide strong evidence that H irradiation is a practical method to passivate defects and thereby enhance the photoresponsivity of $BaSi_2$.

Next, we discuss the SIMS depth profile of H and the secondary ion (Ba + Si) intensities of approximately 300 nm-thick $BaSi_2$ films grown at T_S = 580 °C with various $t_{BaSi:H}$ in the range of 0–30 min, followed by capping with 3 nm-thick pure a-Si layers at T_S = 180 °C. As shown in Fig. 4, the concentration of H atoms increased gradually with $t_{BaSi:H}$, and was uniformly distributed in the samples with $t_{BaSi:H}$ = 9 and 15 min. In the sample with $t_{BaSi:H}$ = 30 min, however, the H concentration was not

uniform. At $t_{BaSi:H}$ = 15 min, the H concentration reached about 1×10^{19} cm^{-3} at depths of 20–320 nm from the surface. This H concentration is higher than that of the sample with $t_{BaSi:H}$ = 0 min, in which the H atoms seem to diffuse from the surface into the deeper bulk region of $BaSi_2$. We cannot distinguish H from H_2 by SIMS. Thus, there is a possibility that H_2 molecules exist in the sample with $t_{BaSi:H}$ = 0 min. This is because H_2 molecules are difficult to evacuate from the ion-pumped MBE chamber. We therefore consider that H_2 molecules might enter $BaSi_2$ films during sample fabrication; however, the defects in $BaSi_2$ were not passivated by H_2, resulting in low photoresponsivity, as shown in Fig. 3.

According to the marked improvement of the photoresponsivity of the atomic H-passivated $BaSi_2$ (sample 3 in Fig. 3), it is reasonable to consider that τ is improved for this sample. In this work, the photoresponsivity of $BaSi_2$ films was measured using the photoconduction effect. Therefore, the photoresponsivity is roughly proportional to the ratio of the carrier lifetime to the carrier transit time [40]. Therefore, we attribute the increase of photoresponsivity to the increase of carrier lifetime and/or the decrease of carrier transit time. To confirm the increase of carrier lifetime, we performed μ-PCD measurements on samples 7, 8, and 9, whose growth conditions were the same as those used for samples 1, 3, and 5, respectively, except for the Si substrate used. For μ-PCD measurements, we used high-ρ FZ-Si substrates instead of low-ρ CZ-Si ones to decrease the microwave intensity reflected from the Si substrate.

Figure 5(a) shows the photoconductivity decay curves of samples 7–9 excited by a pulsed laser intensity of 1.3×10^5 W/cm^2. Assuming that the reflectivity of microwaves is proportional to the excess carrier concentration, we can deduce τ from the decay curves. Electron and holes were generated by the 5-ns laser pulse in a spot with a 2-mm diameter at λ = 349 nm (3.55 eV). The photoconductivity decay was measured from the reflectivity microwave with a frequency of 26 GHz. The estimated areal photon density is $1.3 \times 10^5 \times 5 \times 10^{-9}/(1.6 \times 10^{-19} \times 3.55) \approx 1.1 \times 10^{15}$ cm^{-2}. Assuming that photogenerated carriers are uniformly distributed over the 500 nm-thick H-passivated $BaSi_2$ films (accounting for that the carrier transit time gets much shorter than the carrier life time), the electron–hole pair concentration is calculated to be $1.1 \times 10^{15}/(0.5 \times 10^{-4}) = 2.2 \times 10^{19}$ cm^{-3} on average. The absorption coefficient α at λ = 349 nm is higher than 5×10^5 cm^{-1} [6], and thus the penetration depth of the laser light is $1/\alpha \times 3 \approx$ 60 nm, indicating that most of the photons are absorbed in the H-passivated $BaSi_2$ layer. Here, we define $\tau_{1/e}$ as the time when the reflected microwave intensity decreases by exp(−1) of the initial value after the excitation laser was turned off. As shown in Fig. 5(a), $\tau_{1/e}$ was determined to be approximately 1, 14, and 3 μs for samples 7, 8, and 9, respectively. Note that the measured $\tau_{1/e}$ depends on the thickness of the $BaSi_2$ film, because excess carriers reaching the surface or interface of the samples recombine with

defect states located there. Figure 5(b) compares $\tau_{1/e}$ obtained for samples 8 and 9 in this work as a function of $BaSi_2$ thickness (W) to those reported previously [8]. In our previous work [8], we deduced the carrier lifetime of $BaSi_2$ films from the slope of the decay curves in the time range after the initial rapid decay. In this sense, the $\tau_{1/e}$ values are underestimated in this work compared to those in Ref. [8]. Although the $\tau_{1/e}$ of sample 7 is out of the range, the effect of atomic H passivation of $BaSi_2$ films on carrier lifetime was verified especially in sample 8.

The charge carrier concentrations and Hall mobilities of samples 7–9 were measured at RT with the techniques described elsewhere [41]. The obtained values are: sample 7 ($t_{BaSi:H}$ = 1 min), *p*-type, $p = 1.1 \times 10^{17}$ cm^{-3}, hole mobility μ_p = 25 cm^2/Vs; sample 8 ($t_{BaSi:H}$ = 15 min), *p*-type, $p = 1.8 \times 10^{17}$ cm^{-3}, μ_p = 97 cm^2/Vs; sample 9 ($t_{BaSi:H}$ = 30 min), *n*-type, $n = 9 \times 10^{15}$ cm^{-3}, electron mobility μ_n = 1240 cm^2/Vs. These results reveal that the type of majority carriers changed from holes to electrons as $t_{BaSi:H}$ was increased from 1 to 30 min.

The lattice parameters of $BaSi_2$ films (*a*, *b*, and *c*) in sample 3 were measured to be 8.93, 6.72, and 11.56 Å, respectively. The difference in lattice parameter between sample 3 and reference sample ($t_{BaSi:H}$ = 0 min) was within measurement errors. We also compared the crystalline quality of these samples by the full-width at half maximum values obtained from an x-ray ω–scan rocking curve using a 600 diffraction peak of $BaSi_2$. They were 0.487 and 0.475 °, respectively. On the basis of these results, it is safe to state at least that there is not so much difference in crystalline quality of $BaSi_2$ films between with and without atomic H supply.

C. Theoretical estimates of decay curves

Before starting the theoretical analysis of the experimental data, we present a brief theoretical background of the photoresponse process. A photoresponse is a photoconductivity increase of a sample under irradiation caused by generation of extra charge carriers. The photoconductivity in this case is defined by [42]:

$$\sigma(t) = q\left(\left(n + \Delta n(t)\right)\mu_n + \left(p + \Delta p(t)\right)\mu_p\right), \quad (1)$$

where q is the elementary charge; $\Delta n(t)$ and $\Delta p(t)$, are the time-dependent nonequilibrium electron and hole concentrations, respectively ($\Delta n(t) = \Delta p(t)$); n and p are the equilibrium electron and hole concentrations, respectively. The decrease of photoconductivity after the irradiation is stopped is defined by the decrease of the nonequilibrium charge carrier concentrations over time caused by the recombination processes in semiconductors. The $\Delta n(t)$ and $\Delta p(t)$ dependencies can be found from a

continuity equation, which is in our case has the form [43]

$$\frac{d\Delta n(t)}{dt} = -\sum_i R_i \ , \tag{2}$$

where R_i is the i-th recombination mechanism rate. Actually, at low temperatures like 10 K, very weak photoluminescence (PL) was observed, but it vanished at temperatures higher than 40 K. That is why we consider only nonradiative recombination processes at RT. Thus, the main question is to which excitation(s) in the crystal the energy obtained during recombination will be transferred. The Auger processes become the most favorable for highly nonequilibrium carrier concentrations (usually more than 10^{17} cm^{-3}) [39, 40]. In a general case, the following Auger processes occur: (1) direct band-to-band Auger recombination, (2) phonon-assisted band-to-band Auger recombination, and (3) Auger capture by various traps. Each of these processes has its own recombination rate. Usually (1) or (2) recombination channels are essential either for gapless and narrow gap semiconductors or due to the presence of so called 'resonances' in the band gap structure of the material (which does not occur in the studied system) [43,44]. In fact according to our estimates the recombination rate caused by direct band-to-band Auger recombination and phonon-assisted band-to-band Auger recombination were found to be negligible. Thus, these recombination mechanisms were excluded from further consideration. Therefore, Auger captures by various types of traps were considered to be the main recombination mechanism in our films. However, one also needs to account for that the capture of carriers by traps can be realized through carrier interaction with phonons as well. Usually, such processes are described by the well-known and very general bi- and mono-polar decay rate equation [43]:

$$\frac{d\Delta n}{dt} = -\left(A_{Trap} \cdot N \cdot \Delta n^2 + B_{Trap} \cdot N \cdot \Delta n\right). \tag{3}$$

Here A_{Trap} is the coefficient of Auger capture by traps and N is the trap concentration. Because N cannot be directly obtained or estimated from the experimental data, it is treated as a parameter of the model. A_{Trap} is defined by the expression [44],

$$A_{Trap} = \left(\frac{q^2}{4\pi}\right)^2 \frac{m^*}{\hbar^3}\frac{1}{\varepsilon^2}(4\pi R^2)^3, \tag{4}$$

where ε is the static dielectric constant (14.6 for $BaSi_2$) [5], m^* is the carrier effective mass (0.41 and 0.53 for electrons and holes in $BaSi_2$, respectively, in units of free electron mass) [5], and R is the radius of the trap. R is usually about 10^2 Å for shallow levels and ≤ 10 Å for deep levels in the band gap [44]. A_{Trap} is 9.879 × 10^{-28} and 1.3 ×

10^{-27} cm^6/s for electrons and holes, respectively. B_{Trap} is the capture coefficient for any potential of the attracting center and any mechanism of energy loss. In particular, for the Coulomb potential and the energy relaxation related to the interaction of carriers with phonons, B_{Trap} is defined as [43]

$$B_{Trap} = \frac{(2\pi)^{3/2}\hbar^3}{m^{*3/2}(kT)^{1/2}}\left[\int_0^\infty \frac{\exp\left(\frac{E}{kT}\right)}{C(E)}dE\right]^{-1}, \quad (5)$$

$$C(E) = \frac{4}{3\pi}\frac{m^*}{El}\left(\frac{Zq^2}{\varepsilon\hbar}\right)^3.$$

Here E is the energy, l is the mean free path of carriers ($l = \mu v m^*/q$, where $v = \sqrt{\frac{8kT}{\pi m^*}}$ is the average thermal velocity of carriers), and Zq is the charge of the center (only singly charged centers were considered). Under such assumptions and by solving Eq. (3), the nonequilibrium carrier concentration is defined by

$$\Delta n(t) = \frac{B_{Trap}N\Delta n_0}{A_{Trap}N\Delta n_0 + B_{Trap}N - A_{Trap}N\Delta n_0\exp(-B_{Trap}Nt)}\exp\left(-B_{Trap}Nt\right), \quad (6)$$

where Δn_0 is the steady-state nonequilibrium electron concentration (2.2×10^{19} cm^{-3}) reached during irradiation. The B_{Trap} values for electrons and holes are summarized in Table III.

TABLE III. Theoretical values of B_{Trap} for $BaSi_2$ estimated using Eq. (5).

	B_{Trap} [cm^3/s]	
$t_{BaSi:H}$ [min]	electrons	holes
1	1.304×10^{-9}	5.51×10^{-7}
15	1.911×10^{-8}	1.514×10^{-7}
30	2.861×10^{-9}	5.51×10^{-7}

The experimental data and our theoretical fitting using our generalized approach and treating the trap concentration as a parameter of the model for the normalized photoconductivity versus time for various samples are presented in Fig. 6. N was 6.5×10^{13}, 2.2×10^{12}, and 2.1×10^{13} cm^{-3} for the samples with $t_{BaSi:H}$ = 1, 15, and 30 min,

respectively, which are in good agreement with the previous experimental estimates (~10^{13} cm^{-3}) [20].

The photoconductivity dropped in the initial stage (from 0 to 5 μs) after the irradiation stopped. When the nonequilibrium carrier concentration is high, this drop is mainly defined by the Auger capture of the carriers by various types of traps. The more pronounced decrease in photoconductivity for the samples with $t_{BaSi:H}$ = 1 and 30 min compared with that for the sample with $t_{BaSi:H}$ = 15 min is caused by the higher trap concentrations in the former two samples than in the latter. From 5 to 30 μs, the photoconductivity decrease is defined by the simultaneous influences of Auger capture and phonon-assisted capture of carriers by traps. Thus, the Auger processes initially played a dominant role and then the valuable contribution of the phonon-assisted processes appeared over time because of the decrease of the carrier concentration and, as a consequence, the decrease of the rate of the Auger processes. After 30 μs, the photoconductivity is mainly defined by the phonon-assisted capture of carriers by traps.

D. Theoretical investigation of hydrogen passivation effects

To understand the experimental results along with the theoretical estimates of the trap concentrations, which gave the minimal value for the sample with $t_{BaSi:H}$ = 15 min, one needs to study the possible nature of such traps in detail. Thus, *ab initio* modeling of various $BaSi_2$ structures with V_{Si} and incorporated H atoms was performed.

$BaSi_2$ crystallizes with a simple orthorhombic structure (space group *Pnma*) and has lattice parameters of a = 8.942 Å, b = 6.733 Å, and c = 11.555 Å [45]. In a $BaSi_2$ crystal, 8 Ba and 16 Si atoms are grouped into two and three chemically inequivalent sites, respectively (see Fig.1). A structural feature of this crystal structure is the presence of slightly distorted isolated Si_4 tetrahedra that act as anions in the sublattice of Ba atoms, which can be viewed as cations [45]. This structural feature indicates the mostly ionic nature of the chemical bonding in a $BaSi_2$ crystal, although covalent bonding prevails within Si_4 tetrahedra [22,25].

Thin films of $BaSi_2$ contain grain boundaries, which can be considered as a primary site of H incorporation. An *ab initio* study of $BaSi_2$ monocrystalline thin films with different orientations indicated the presence of some surface-localized states within the gap when Si_4 tetrahedra were present on the surface, whereas Ba surface termination resulted in lower surface energies and the absence of surface-localized states [25]. In addition, both Ba and Si vacancies are not excluded on the surface providing there is enough room for H to saturate dangling bonds. Unfortunately, it is not yet possible to model real grain boundaries because of their numerous structural variants. However, $BaSi_2$ grains are rather large (~0.2 μm on average) [41] with respect to the grain boundary area and we can consider the bulk of $BaSi_2$ to absorb most of H. In bulk $BaSi_2$,

H can occupy a V_{Si} or enter an interstice (the $BaSi_2$ unit cell with Si_4 tetrahedra is shown in Fig. 1). In the former case, three H atoms are necessary to formally saturate all dangling bonds in the tetrahedron with one removed Si atom. Moreover, an enlarged unit cell is necessary for simulations to prevent a sizable defect–defect interaction since even in our enlarged unit cell the defect concentration is larger than 10^{20} cm^{-3}.

Optimization of the ideal $BaSi_2$ crystal structure resulted in lattice parameters (a = 9.040 Å, b = 6.766 Å, and c = 11.594 Å) which were very close to the experimental ones (both for bulk [45] and our grown thin films). Any structural variant of $BaSi_2$ with V_{Si} and/or with H incorporation did not show significant changes in the lattice parameters (the maximal difference did not exceed 0.2 %) in accordance with our experimental data. Moreover, we found valuable changes only in a Si_4 tetrahedron with V_{Si}: the Si-Si interatomic distances got shorter (2.33 – 2.39 Å to be compared to 2.41 – 2.45 Å for the ordinary Si_4 tetrahedron). Such distortion could be viewed to be local because it did not affect atomic positions of the other atoms. In addition, since there was enough space to use several H atoms to saturate dangling bonds in the case of V_{Si}, H incorporation caused again local distortion. The corresponding calculated DOS of $BaSi_2$ with one V_{Si} along with the cases of incorporation of one, two, and three H atoms to passivate dangling bonds in a tetrahedron are shown in Fig. 7. First of all we would like to point out that there are no sizable changes in the band-gap value, in the structure of the valence and conduction bands as well as in the character of the states which define different hybridizations of bonding states in the valence band and antibonding states in the conduction band with respect to the ideal $BaSi_2$ structure [5]. Usually the appearance of point defects in an ideal structure provides additional energy levels (or low-dispersed bands) in the gap region associated with these defects. And in its turn they could lead to the drastic changes in the transport properties as well as in some dynamical characteristics of relaxation processes of the system under consideration. So let us study these changes more in detail for our material. In the case of $BaSi_2$ with V_{Si} it is evident that the V_{Si} causes a localized state consisting of two energy bands to appear close to the middle of the band gap. This localized state is half filled, which originates from p states of Si atoms belonging to the tetrahedron with the removed Si atom and acts as a trap. One H atom can saturate only one dangling bond of the Si atom in the tetrahedron with the V_{Si}. In this case, there is one half-filled energy band in the localized state, which leads to a decrease of the trap concentration. If two H atoms saturate dangling bonds, the completely filled localized state (consisting of one energy band, which is characterized by p states of the one remaining Si atom with a dangling bond) shifts towards the top of the valence band and acts as a deep donor level. Incorporation of a third H provided complete termination of all dangling bonds and led to degenerate semiconducting properties because the Fermi level was in the conduction band,

equivalent to the scenario if one electron was added to the system. We found two distinct variants in the case of an interstitial H atom in the $BaSi_2$ unit cell (see Fig. 8). The first one [Fig. 8 (a)] is very similar to the case of three H atoms and V_{Si} with degenerate semiconducting properties. It corresponds to the case when the first neighbor of H is a Ba atom. The second one [Fig. 8(b)] occurs if the first neighbor of H is a Si atom and suggests formation of a trap in the middle of the gap because it has a half-filled localized state originating from H *s*, Si *p*, and Ba *d* states (these Si and Ba atoms are located very close to the H atom).

It should be stressed that all the studied structures can statistically occur in the systems under consideration. Therefore, the structure of the sample fabricated with $t_{BaSi:H}$ = 1 min can be characterized mainly by the presence of the cases represented in Fig. 7(a) and (b) (i.e., only the V_{Si} and a V_{Si} with one H-saturated dangling bond, respectively). This situation leads to a high trap concentration. As the concentration of incorporated H was increased, the structure of the sample fabricated with $t_{BaSi:H}$ = 15 min may be defined mainly by the cases represented in Fig. 7(c) (the V_{Si} with two H-saturated dangling bonds), which in turn leads to a considerable decrease of the trap concentration. Finally, when the H concentration is maximal, like in the sample fabricated with $t_{BaSi:H}$ = 30 min, the structure is characterized by the cases represented in Fig. 7(d) and Fig. 8 (three H completely passivate all dangling bonds of the V_{Si} and an ideal $BaSi_2$ crystal with one H in an interstice, respectively). On the one hand, the maximum H concentration leads to the change of the major charge carrier [Fig. 7(d) and Fig. 8(a)] and, on the other hand, to an increase of the trap concentration [Fig. 8(b)]. Unfortunately, the experimentally determined trap concentration value of about 10^{13} cm^{-3} cannot be treated directly by *ab initio* calculations because of the serious limitations on the size of the considered systems. In the enlarged unit cell we used for calculations the minimal defect concentration cannot be less that 10^{20} cm^{-3} indicating that it is impossible to completely attenuate the defect-defect interaction. As a result, localized bands with very low dispersion appear in the energy gap region due to interaction of Si atoms with dangling bonds in a tetrahedron with V_{Si}. However, in the direct space everything is localized within the area of a tetrahedron with V_{Si} indicating that our *ab initio* analysis are correct and can only help one to understand qualitatively the influence of H incorporation into $BaSi_2$ on its properties.

IV. CONCLUSION

First, we confirmed the optimal growth conditions of an a-Si:H passivation layer on $BaSi_2$. Based on the photoresponse spectra, $t_{a\text{-}Si:H}$ of 15 min and T_S of 180 °C were found to be optimal. The results also indicated that the properties of a-Si:H are sensitive to the growth conditions. This is the first time $BaSi_2$ films have been passivated using

atomic H, and we obtained the highest photoresponsivity ever reported for $BaSi_2$. H atoms are considered to occupy V_{Si} and passivate point defects in $BaSi_2$. Our μ-PCD measurements confirmed that τ of $BaSi_2$ films was lengthened following H passivation. To explain the experimentally obtained photoconductivity decay curves, various trap-related recombination mechanisms were considered. In the initial stage after the irradiation was stopped, the Auger processes played a dominant role and then the contribution of the phonon-assisted processes became more pronounced over time because of the decreases of the carrier concentration and rate of Auger processes. Trap concentrations were shown to be 6.5×10^{13}, 2.1×10^{13}, and 2.2×10^{12} cm^{-3} in the samples fabricated with $t_{BaSi:H}$ = 1, 30, and 15 min, respectively. These estimates are in good agreement with previous experimental results (of the order of 10^{13} cm^{-3}) [20]. Such variations in the trap concentrations along with the change of the type of majority carrier from holes to electrons as $t_{BaSi:H}$ was lengthened from 1 to 30 min were qualitatively explained by our results obtained from *ab initio* electronic property simulations of $BaSi_2$ with V_{Si} and H incorporation.

Acknowledgments

This work was financially supported by a Grant-in-Aid for Scientific Research A (Grant No. 18H014477) from the Japan Society for the Promotion of Science (JSPS) and by the Belarusian National Research Programs “Convergence 2020”, “Materials Science, New Materials and Technology” from the Belarusian Republican Foundation for Fundamental Research (Grant No. F18MC-012).

[1] T. D. Lee and A. U. Ebong, Renew. Sust. Energ. Rev. **70,** 1286 (2017).
[2] T. Suemasu, Jpn. J. Appl. Phys. **54,** 07JA01 (2015).
[3] T. Suemasu and N. Usami, J. Phys. D. Appl. Phys. **50,** 023001 (2017).
[4] K. Morita, Y. Inomata, and T. Suemasu, Thin Solid Films **508**, 363 (2006).
[5] D. B. Migas, V. L. Shaposhnikov, and V. E. Borisenko, Phys. Status Solidi (b) **244**, 2611 (2007).
[6] K. Toh, T. Saito, and T. Suemasu, Jpn. J. Appl. Phys. **50**, 068001 (2011).
[7] M. Kumar, N. Umezawa, and M. Imai, Appl. Phys. Express **7**, 071203 (2014).
[8] K. O. Hara, N. Usami, K. Nakamura, R. Takabe, M. Baba, K. Toko, and T. Suemasu, Appl. Phys. Express **6**, 112302 (2013).
[9] M. Baba, M. Kohyama, and T. Suemasu, J. Appl. Phys. **120**, 085311 (2016).
[10] R. A. McKee, F. J. Walker, J. R. Conner, E. D. Specht, and D. E. Zelmon, Appl. Phys. Lett. **59**, 782 (1991).
[11] R. A. McKee, F. J. Walker, J. R. Conner, and R. Raj, Appl. Phys. Lett. **63**, 2818 (1993).
[12] K. Morita, M. Kobayashi, and T. Suemasu, Jpn. J. Appl. Phys. **45**, L390 (2006).
[13] Y. Imai and A. Watanabe, Intermetallics **18**, 1432 (2010).
[14] S. Yachi, R. Takabe, H. Takeuchi, K. Toko, and T. Suemasu, Appl. Phys. Lett. **109**, 072103 (2016).
[15] T. Deng, T. Sato, Z. Xu, R. Takabe, S. Yachi, Y. Yamashita, K. Toko, and T. Suemasu, Appl. Phys. Express **11**, 062301 (2018).
[16] T. Suemasu, K. Morita, M. Kobayashi, M. Saida, and M. Sasaki, Jpn. J. Appl. Phys. 45, L519 (2006).
[17] K. Kodama, R. Takabe, T. Deng, K. Toko, and T. Suemasu, Jpn. J. Appl. Phys. **57**, 050310 (2018).
[18] K. Kodama, Y. Yamashita, K. Toko, and T. Suemasu, Appl. Phys. Express **12**, 041005 (2019).
[19] R. Takabe, T. Deng, K. Kodama, Y. Yamashita, T. Sato, K. Toko, and T. Suemasu, J. Appl. Phys. **123,** 045703 (2018).
[20] Y. Yamashita, T. Sato, M. Emha Bayu, K. Toko, and T. Suemasu, Jpn. J. Appl. Phys. **57**, 075801 (2018).
[21] S. M. Kauzlarich, Chemistry, Structure and Bonding of Zintl Phases and Ions, Wiley-VCH, 199.
[22] M. Kumar, N. Umezawa, W. Zou, and M. Imai, J. Mater. Chem. A **5**, 25293 (2017).
[23] S. Okasaka, O. Kubo, D. Tamba, T. Ohashi, H. Tabata, and M. Katayama, Surf. Sci. **635**, 115 (2015).
[24] O. Kubo, T. Otsuka, S. Okasaka, S. Osaka, H. Tabata, and M. Katayama, Jpn. J.

Appl. Phys. **55**, 08NB11 (2016).
[25] D. B. Migas, V. O. Bogorodz, A. V. Krivosheeva, V. L. Shaposhnikov, A. B. Filonov, V. E. Borisenko, Jpn. J. Appl. Phys. **56**, 05DA03 (2017).
[26] F. T. Dittrich, Materials Concepts for Solar Cells (Imperial College Press, London, 2015) Chaps 3 and 9.
[27] M. Taguchi, A. Terakawa, E. Maruyana, and M. Tanaka, Prog. Photovol.: Res. Appl. **13**, 481 (2005).
[28] Y. Tsunomura, Y. Yoshimine, M. Taguchi, T. Baba, T. Kinoshita, H. Kanno, H. Sakata, E. Maruyama, and M. Tanaka, Sol. Energ. Mater. Sol. Cells **93**, 670 (2009).
[29] R. Takabe, S. Yachi, W. Du, D. Tsukahara, H. Takeuchi, K. Toko, and T. Suemasu, AIP Adv. 6, 085107 (2016).
[30] Z. Xu, K. Gotoh, T. Deng, T. Sato, R. Takabe, K. Toko, N. Usami, and T. Suemasu, AIP Adv. **8,** 055306 (2018).
[31] J. B. Nelson and D. P. Riley, Proc. Phys. Soc. **57**, 160 (1945).
[32] G. Kresse and J. Hafner, Phys. Rev. B **49**, 14251 (1994).
[33] G. Kresse and J. Furthmüller, Phys. Rev. B **54**, 11169 (1996).
[34] G. Kresse and J. Joubert, Phys. Rev. B **59**, 1758 (1999).
[35] J. P. Perdew, S. Burke, and M. Ernzerhof, Phys. Rev. Lett. **77**, 3865 (1996).
[36] S. Sriraman, S. Agarwal, E. S. Aydil, and D. Maroudas, Nature **418**, 62 (2002).
[37] H. Fujiwara and M. Kondo, Appl. Phys. Lett. **90,** 013503 (2007).
[38] H.-J. Lin and S.-H. Chen, Opt. Mater. Express **3,** 1215 (2013).
[39] A. Hara, Jpn. J. Appl. Phys. **46,** 962 (2007).
[40] S. M. Sze, Physics of Semiconductor Devices, 2nd ed., John Wiley & Sons, 1981.
[41] T. Deng, T. Suemasu, D. A. Shohonov, I. S. Samusevich, A. B. Filonov, D. B. Migas, and V. E. Borisenko, Thin Solid Films **661**, 7 (2018).
[42] R. H. Bube, Photoconductivity of Solids, Wiley, New York, 1960.
[43] V. N. Abakumov, V. I. Perel, and I. N. Yassievich, Nonradiative recombination of semiconductors, North Holland, 1991.
[44] B.K. Ridley, Quantum Processes in Semiconductors, Clarendon Press, Oxford, 1982.
[45] J. Evers, J. Solid State Chem. **32**, 77 (1980).

Figure captions

FIG. 1. Crystal structure of orthorhombic $BaSi_2$. There are three inequivalent Si sites and two inequivalent Ba sites.

FIG. 2 (a) Photoresponsivity spectra of 500 nm-thick $BaSi_2$ layers capped with approximately 3 nm-thick a-Si:H fabricated with various $t_{a\text{-}Si:H}$. (b) Photoresponsivity spectra of 500 nm-thick $BaSi_2$ layers capped with approximately 3 nm-thick a-Si:H fabricated with various T_S.

FIG. 3. Photoresponsivity spectra of 500 nm-thick $BaSi_2$ layers passivated by atomic H with various values of $t_{BaSi:H}$ in the range of 0–30 min.

FIG. 4. SIMS depth profiles of H atoms of approximately 300 nm-thick $BaSi_2$ films with various values of $t_{BaSi:H}$ in the range of 0–30 min at T_S = 580 °C. Depth profiles of ions (Ba and Si) of $BaSi_2$ films with $t_{BaSi:H}$ = 15 min is also shown.

FIG. 5. (a) Photoconductivity decay curves of atomic H-passivated $BaSi_2$ films in samples 7-9, fabricated using different $t_{BaSi:H}$. (b) Comparison of τ obtained for samples 8 and 9 as a function of $BaSi_2$ thickness W to those reported previously [8].

FIG. 6. Normalized photoconductivity of $BaSi_2$ versus time. Comparison of experimental data (samples 7-9) with theoretical estimations obtained by the approach using Eqs. (1), (4), (5) and (6). Photoconductivity is normalized to the value at t = 0.

FIG. 7. Total density of states of enlarged $BaSi_2$ unit cells with (a) one Si vacancy, (b) one H atom in a Si vacancy, (c) two H atoms in a Si vacancy, and (d) three H atoms in a Si vacancy. The vertical dashed line indicates the Fermi level.

FIG. 8. Total density of states of an enlarged $BaSi_2$ unit cell with one H in different interstitial positions indicating (a) degenerate semiconducting properties and (b) the appearance of a trap in the gap region.

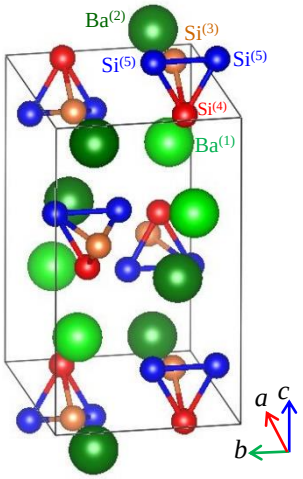

FIG. 1. Crystal structure of orthorhombic $BaSi_2$. There are three inequivalent Si sites and two inequivalent Ba sites.

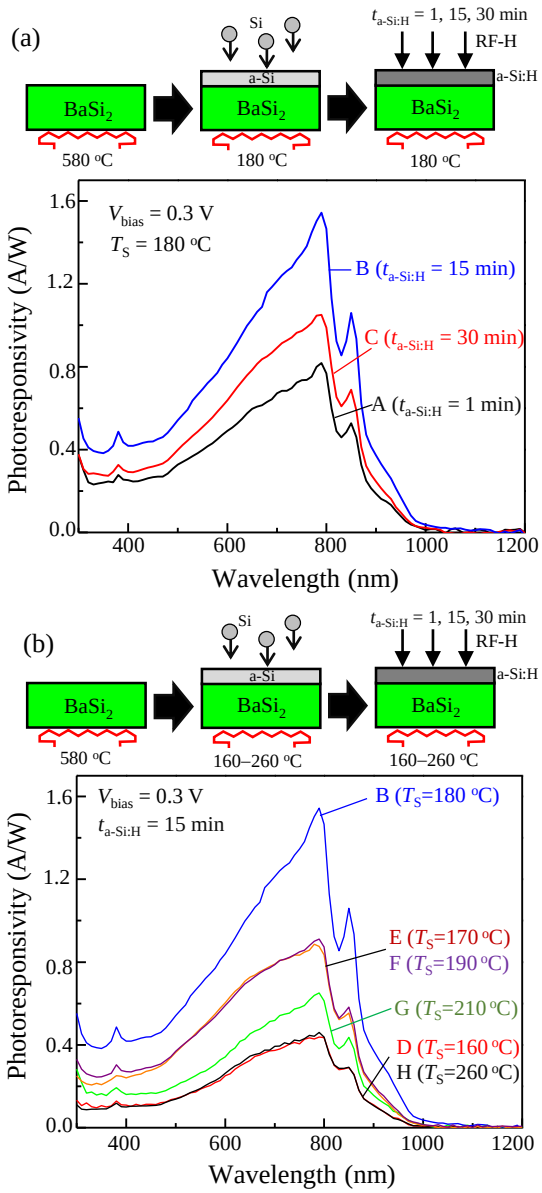

FIG. 2 (a) Photoresponsivity spectra of 500 nm-thick $BaSi_2$ layers capped with approximately 3 nm-thick a-Si:H fabricated with various $t_{a\text{-}Si:H}$. (b) Photoresponsivity spectra of 500 nm-thick $BaSi_2$ layers capped with approximately 3 nm-thick a-Si:H fabricated with various T_S.

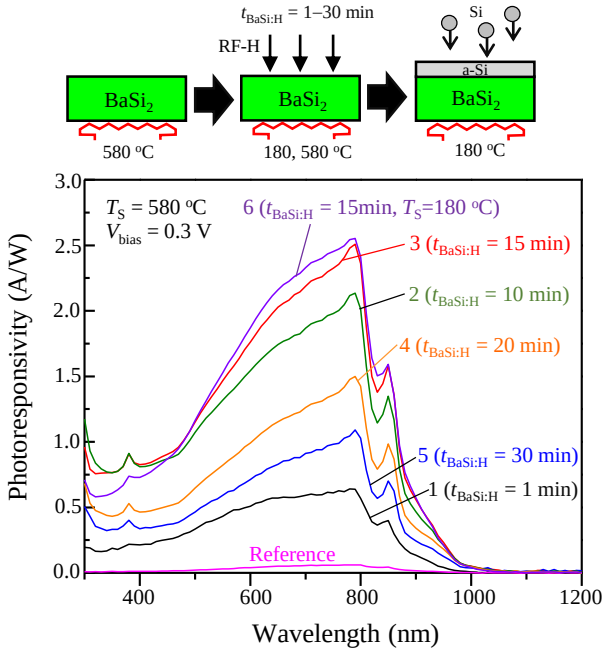

FIG. 3. Photoresponsivity spectra of 500 nm-thick $BaSi_2$ layers passivated by atomic H with various values of $t_{BaSi:H}$ in the range of 0–30 min.

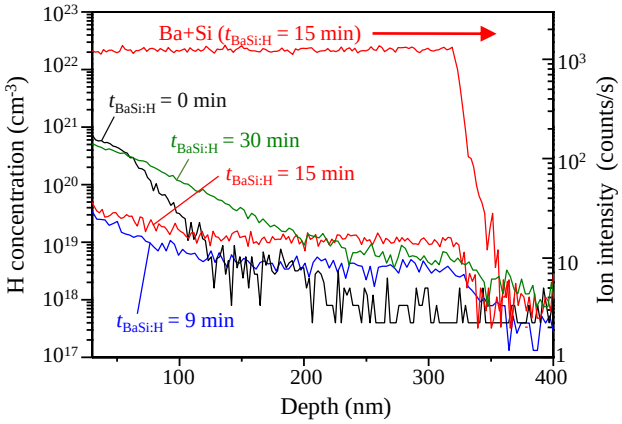

FIG. 4. SIMS depth profiles of H atoms of approximately 300 nm-thick $BaSi_2$ films with various values of $t_{BaSi:H}$ in the range of 0–30 min at T_S = 580 °C. Depth profiles of ions (Ba and Si) of $BaSi_2$ fims with $t_{BaSi:H}$ = 15 min is also shown.

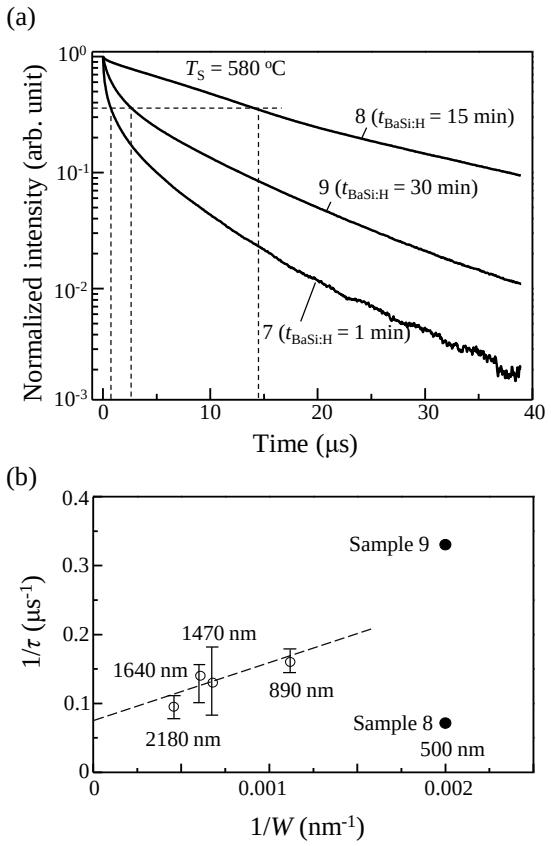

FIG. 5. (a) Photoconductivity decay curves of atomic H-passivated $BaSi_2$ films in samples 7-9, fabricated using different $t_{BaSi:H}$. (b) Comparison of τ obtained for samples 8 and 9 as a function of $BaSi_2$ thickness W to those reported previously [8].

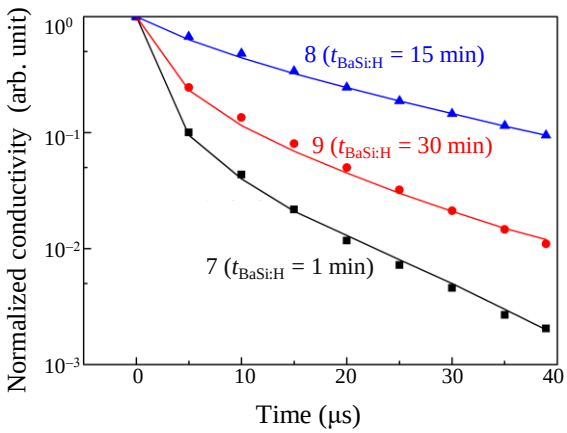

FIG. 6. Normalized photoconductivity of $BaSi_2$ versus time. Comparison of experimental data (samples 7-9) with theoretical estimations obtained by the approach using Eqs. (1), (4), (5) and (6). Photoconductivity is normalized to the value at $t = 0$.

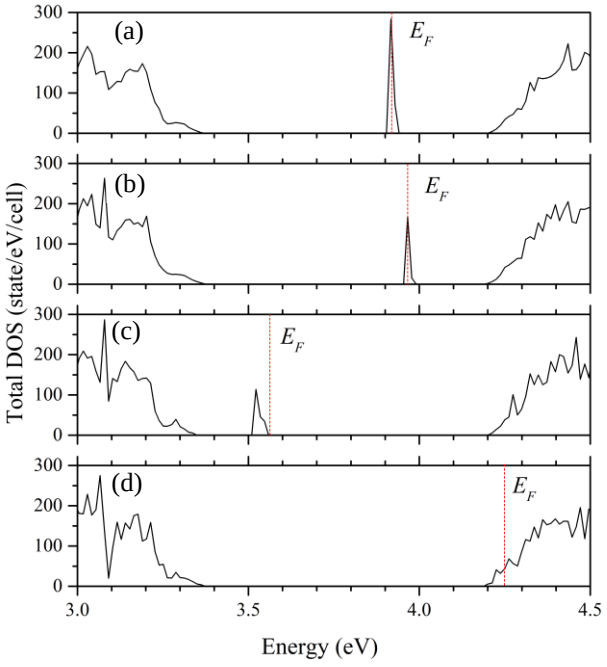

FIG. 7. Total density of states of enlarged $BaSi_2$ unit cells with (a) one Si vacancy, (b) one H atom in a Si vacancy, (c) two H atoms in a Si vacancy, and (d) three H atoms in a Si vacancy. The vertical dashed line indicates the Fermi level.

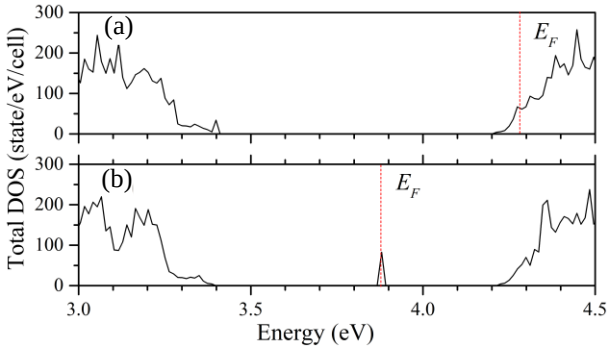

FIG. 8. Total density of states of an enlarged $BaSi_2$ unit cell with one H in different interstitial positions indicating (a) degenerate semiconducting properties and (b) the appearance of a trap in the gap region.